ADVANCED SCIENCE NEWS
www.advancedsciencenews.com

Inhibiting Solid Tumor Growth In Vivo by Non-Tumor-Penetrating Nanomedicine

Shixian Lv, Zhaohui Tang, Wantong Song, Dawei Zhang, Mingqiang Li, Huaiyu Liu, Jianjun Cheng, Wu Zhong,* and Xuesi Chen**

***N**anomedicine (NM) cannot penetrate deeply into solid tumors, which is partly attributed to the heterogeneous microenvironment and high interstitial fluid pressure of solid tumors. To improve NM efficacy, there has been tremendous effort developing tumor-penetrating NMs by miniaturizing NM sizes or controlling NM surface properties. But progress along the direction of developing tumor penetrating nanoparticle has been slow and improvement of the overall antitumor efficacy has been limited. Herein, a novel strategy of inhibiting solid tumor with high efficiency by dual-functional, nontumor-penetrating NM is demonstrated. The intended NM contains 5,6-dimethylxanthenone-4-acetic acid (DMXAA), a vascular-disrupting agent, and doxorubicin (DOX), a cytotoxic drug. Upon arriving at the target tumor site, sustained release of DMXAA from NMs results in disruption of tumor vessel functions, greatly inhibiting the interior tumor cells by cutting off nutritional supply. Meanwhile, the released DOX kills the residual cells at the tumor exterior regions. The in vivo studies demonstrate that this dual-functional, nontumor penetrating NM exhibits superior anticancer activity, revealing an alternative strategy of effective tumor growth inhibition.*

Dr. S. Lv, Dr. Z. Tang, Dr. W. Song, D. Zhang, Dr. M. Li, Prof. X. Chen
Key Laboratory of Polymer Ecomaterials
Changchun Institute of Applied Chemistry
Chinese Academy of Sciences
Changchun 130022, China
E-mail: xschen@ciac.ac.cn
H. Liu
Laboratory Animal Center
Jilin University
Changchun 130012, China
Prof. J. Cheng
Department of Materials Science and Engineering
University of Illinois at Urbana-Champaign
Urbana, IL 61801, USA
E-mail: jianjunc@illinois.edu
Prof. W. Zhong
Laboratory of Computer-Aided Drug Design and Discovery
Beijing Institute of Pharmacology and Toxicology
Beijing 100850, China
E-mail: zhongwu@bmi.ac.cn

DOI: 10.1002/smll.201600954

1. Introduction

Nanoparticle (NP) containing chemotherapeutic agent has recently emerged as a new anticancer modality, which can potentially provide the treatment of cancer with higher efficiency and lower toxicity compared to conventional chemotherapy.[1–11] It is generally believed that NPs capable of deeper tumor penetration and more protracted retention should have better anticancer efficacy. Although progress has been made using model anticancer NPs with moderate tumor penetration capability in several fundamental studies, NPs with sufficient tumor-penetration capacity that can be of practical use are yet to be developed.[12–16] Current nanomedicines (NMs) can effectively kill cancer cells at or near the periphery of solid tumors but cannot reach the interior area to eliminate inner malignant cells, due in part to the heterogeneous microenvironment and elevated interstitial fluid pressure in tumor tissues.[12,17,18] Herein, we report the demonstration of the effective suppression of solid tumor growth with specially designed, dual-functional NPs that even stay largely on the margin of the solid tumors.

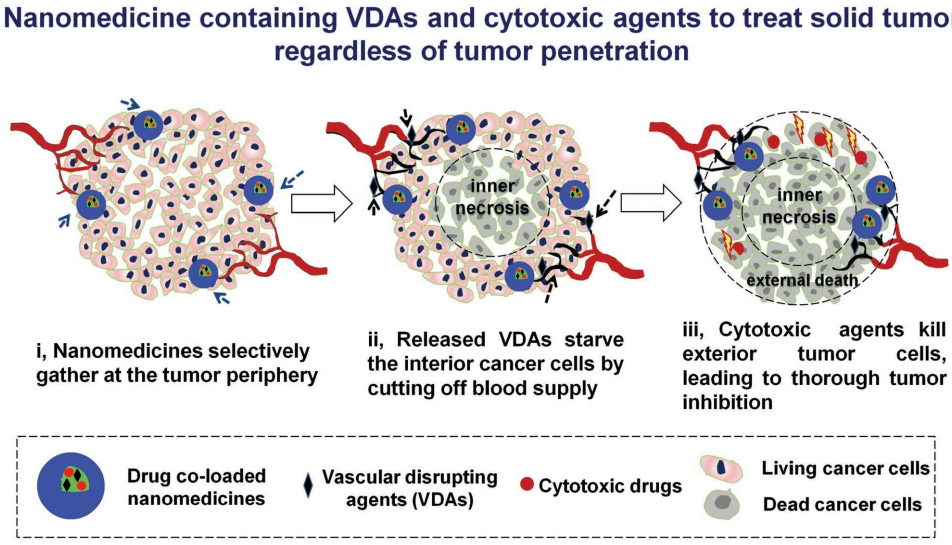

Scheme 1. Schematic illustration of cancer treatment by NM containing a VDA and a cytotoxic agent in treating solid tumor.

The growth of solid tumor is accompanied and facilitated by angiogenesis.[17,19,20] Disrupting the blood flow and nutrient supply to solid tumors has been validated effective to inhibit tumor growth. Vascular disrupting agents (VDAs), a special class of vascular targeting agents, are able to selectively disrupt the newly formed and immature tumor vasculature, deprive the blood and nutrient supply to inner tumor cells, and lead to extensive central necrosis.[21–23] While small-molecule VDAs usually have large distribution volumes after systemic administration, NPs tend to have better tumor accumulation capability because of the well-known enhanced permeation and retention (EPR) effect.[24–27] Thus, NPs may effectively accumulate the small-molecule VDAs at tumor site when used as delivery vehicles and achieve enhanced tumor vascular disrupting activity. Furthermore, although VDAs are effective to induce severe necrosis to the poorly vascularized central tumor regions, a thin layer of viable tumor cells is inevitably found near the highly vascularized tumor periphery.[28–32] A possible reason is that these exterior tumor cells can acquire sufficient nutrients from the nearby blood vessels of normal tissues, which are generally insensitive to VDAs. Given that the residual rim of highly proliferative and well-nourished cells can serve as a source of tumor regrowth, treatment of tumor by VDA alone is unlikely to eradicate the entire solid tumor.

We hypothesize that NPs codelivering a VDA and a conventional chemotherapeutic agent to the tumor site and controlling the local release of these therapeutic agents may effectively inhibit tumor growth even if the NPs have low tumor tissue penetration. Such dual-agent containing NP with each drug playing its intended function, the VDA to starve the interior cancer cells and the chemotherapeutic agent to kill the cancer cells in the exterior layer of solid tumor, may provide a practical formulation for effective tumor growth inhibition (**Scheme 1**). To validate this hypothesis, we designed a polypeptide-based NP containing both agents. We synthesized methoxy poly(ethylene glycol)-*b*-poly-[(*N*-2-hydroxyethyl)-aspartamide] (mPEG-*b*-PHEA), for covalent conjugation of 5,6-dimethylxanthenone-4-acetic acid (DMXAA), a potent tumor-VDA, to first prepare mPEG-*b*-PHEA-DMXAA conjugate (PPD) and then utilized PPD for the encapsulation of doxorubicin (DOX), a chemotherapeutic drug.

In this study, we report the preparations and characterizations of PPD and DOX encapsulated PPD (DOX-PPD). We then report the tumor distributions of the designed NPs and delivered drugs, and the antitumor efficacy of the dual-agent containing NP in a subcutaneous transplanted tumor model of human breast cancer.

2. Results and Discussion

2.1. Preparations and Characterizations of PPD and DOX-PPD

The preparations for PPD and DOX-PPD were described in **Scheme 2**. A well-defined polymer, mPEG-*b*-PHEA, based on poly(ethylene glycol)-*b*-poly(amino acid) (PEG-PAA) was first synthesized for the conjugation of DMXAA. We chose PEG-PAA as the vehicle material because of the excellent biocompatibility and good biodegradability of the polypeptide block.[33–35] mPEG-*b*-PHEA was synthesized through the ring opening polymerization (ROP) of γ-benzyl-L-aspartate-*N*-carboxyanhydride (BLA-NCA) monomer as initiated by mPEG-NH_2 at the amine/NCA ratio of 14, followed by ammonolysis with ethanolamine. The structures of mPEG-*b*-poly(γ-benzyl-L-aspartate) (mPEG-*b*-PBLA) and mPEG-*b*-PHEA were confirmed by ^{1}H NMR (Figure S1, Supporting Information). The aspartic acid units in mPEG-*b*-PBLA and mPEG-*b*-PHEA copolymers calculated from ^{1}H NMR were both 12, suggesting the good stability of poly(aspartic acid) backbone during ammonolysis process. Gel permeation chromatography (GPC) analysis demonstrated the narrow molecular weight distributions of both mPEG-*b*-PBLA and mPEG-*b*-PHEA copolymers (polydispersity index, PDI = 1.06 and 1.18, respectively, Figure S2, Supporting Information). DMXAA was conveniently conjugated

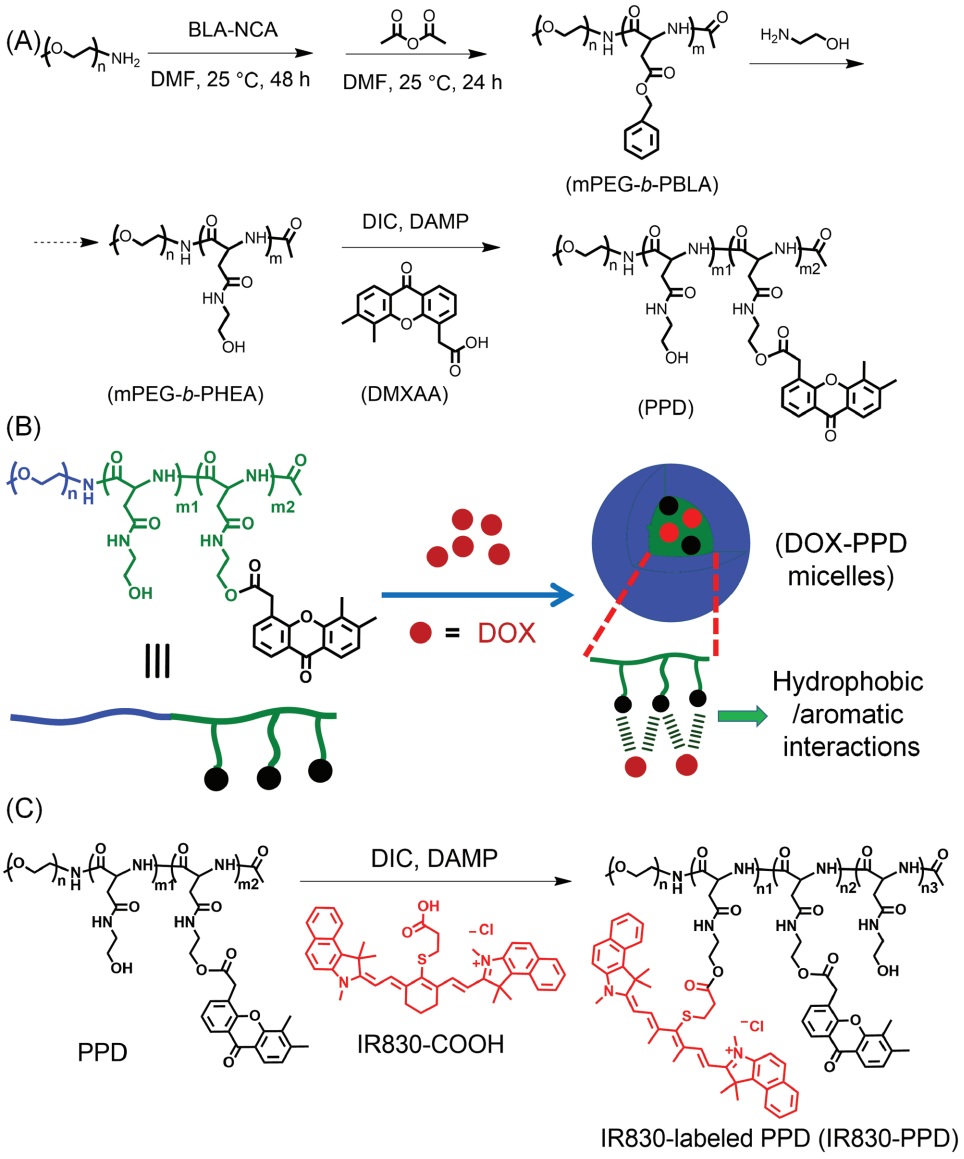

Scheme 2. A) Preparations of PPD, B) DOX-PPD, and C) IR830-labeled PPD (IR830-PPD).

to mPEG-*b*-PHEA and the efficient conjugation was confirmed by ^{1}H NMR and fourier transform infrared (FT-IR) analyses (Figures S3 and S4, Supporting Information). UV analysis indicated no change of DMXAA chemical structure (Figure S5, Supporting Information). Fairly high loading of DMXAA in the DMXAA-mPEG-*b*-PHEA conjugate was achieved (11.8%).

After bonding of hydrophobic DMXAA, amphiphilic PPD could self-assemble into micelles. DOX was successfully encapsulated into the PPD micelles through hydrophobic/π–π interactions with DMXAA (Scheme 2B). The DOX content in DOX-PPD was 5.4%, with a loading efficiency of 82.6%. The sizes and morphologies of PPD and DOX-PPD micelles were studied by dynamic laser scattering (DLS) and transmission electron microscopy (TEM), respectively. The hydrodynamic radii of PPD and DOX-PPD micelles determined by DLS were 18.7 ± 3.4 and 31.5 ± 9.4 nm (**Figure 1**A), respectively. TEM images confirmed the uniformly spherical morphologies of PPD and DOX-PPD (Figure 1B). The suitable sizes of PPD and DOX-PPD should facilitate their accumulation in solid tumor via EPR effect as they are large enough to avoid filtration by the kidney (R_h > 10 nm) and small enough to avoid a specific sequestration by sinusoids in spleen and fenestra of liver (R_h < 50 nm).[36] The surface charges of PPD and DOX-PPD micelles were nearly neutral (≈–3 mV, Table S1, Supporting Information). The blood stabilities of PPD and DOX-PPD micelles were evaluated in phosphate buffered saline (PBS) medium with 10% fetal bovine serum (FBS). Both PPD and DOX-PPD micelles could maintain their sizes for at least 72 h in serum-containing media (Figure 1C,D), revealing their excellent blood stabilities.

The release of DMXAA from PPD was studied in PBS. As expected, sustained DMXAA release pattern was observed because of the covalent ester linkage between DMXAA and mPEG-*b*-PHEA (Figure 1E). Although DMXAA and other

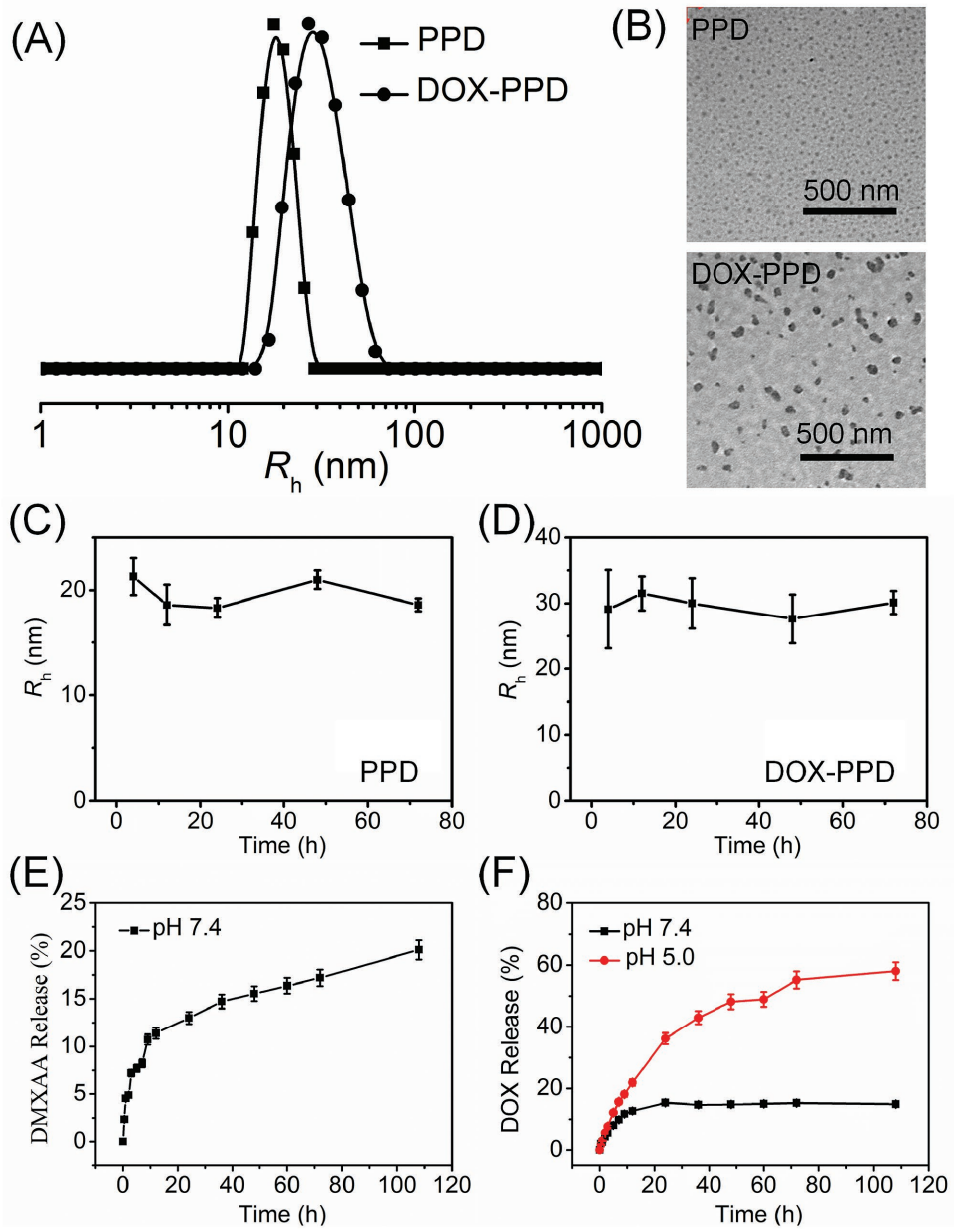

Figure 1. A) Hydrodynamic radii and B) typical morphologies of PPD and DOX-PPD measured by DLS and TEM. Hydrodynamic radius changes of C) PPD and D) DOX-PPD after incubation with PBS containing 10% FBS at 37 °C. In vitro E) DMXAA release from PPD and F) DOX release from DOX-PPD in PBS.

tumor-VDAs can cause rapid suppression to tumor blood vasculature with maximal vessel collapse at 1–6 h postinjection,[37,38] investigations on the real-time response of solid tumors to VDA treatment revealed that VDA-mediated collapse of tumor vessels was time-dependent and transient. Because of the overexpression of pro-angiogenic factors, tumor tissues may still undergo extensive vascular remodeling and vigorous neovascularization at a low concentration of VDA,[39] substantiating the importance of protracted local retention of VDA for sustained antiangiogenic effect. While small-molecule VDAs are unlikely to localize in tumor tissue for extended period of time to display permanent tumor vascular damage due to their very large volume distribution and rapid blood/tumor clearance, PPD is designed to have more efficient accumulation and protracted retention at the tumor tissue by EPR effect. Thus after PPD accumulating at the tumor site, sustained DMXAA release from PPD would lead to extended tumor vascular disrupting activity and enhanced antitumor effect. The release of DOX from DOX-PPD was found to be sensitive to pH changes (Figure 1F), which might be attributed to the protonable amino groups on DOX. The increased hydrophilicity of DOX at acidic condition will weaken the hydrophobic/π–π interactions between DOX and DMXAA, resulting in fast DOX release. Such design ensures negligible DOX release during circulation until the DOX-PPD reaches acidic tumor tissue or is internalized to acidic endolysosomal compartments of the targeted cancer cells.[40]

2.2. In Vitro Cytotoxicity and Cell Uptake Studies

The cytotoxicities of mPEG-*b*-PHEA and different drug formulations were investigated by 3-(4,5-dimethyl-thiazol-2-yl)-2,5-diphenyl tetrazolium bromide (MTT) assay. As shown in Figure S6 (Supporting Information), the viabilities of A549, MCF-7, and NIH/3T3 cells incubated with the mPEG-*b*-PHEA at all the designed concentrations up to 1000 μg mL^{-1} were above 85%, demonstrating the excellent biocompatibility of the polymer. According to the literature, DMXAA is not cytotoxic to cancer cells, and the antitumor activity of DMXAA is attributed largely to its vascular disrupting ability.[41] Therefore, it was not surprising to observe that both free DMXAA and PPD micelles were practically nontoxic to A549 and MCF-7 cells (Figure S7A, Supporting Information and **Figure 2**A). In addition, PPD showed minimal cytotoxicity to normal cells (NIH/3T3). DOX-PPD micelles exhibited obvious cytotoxicity to both tumorous and nontumorous cells (Figure S7, Supporting Information and Figure 2B). The results also showed that DOX-PPD appeared to have similar cell proliferation

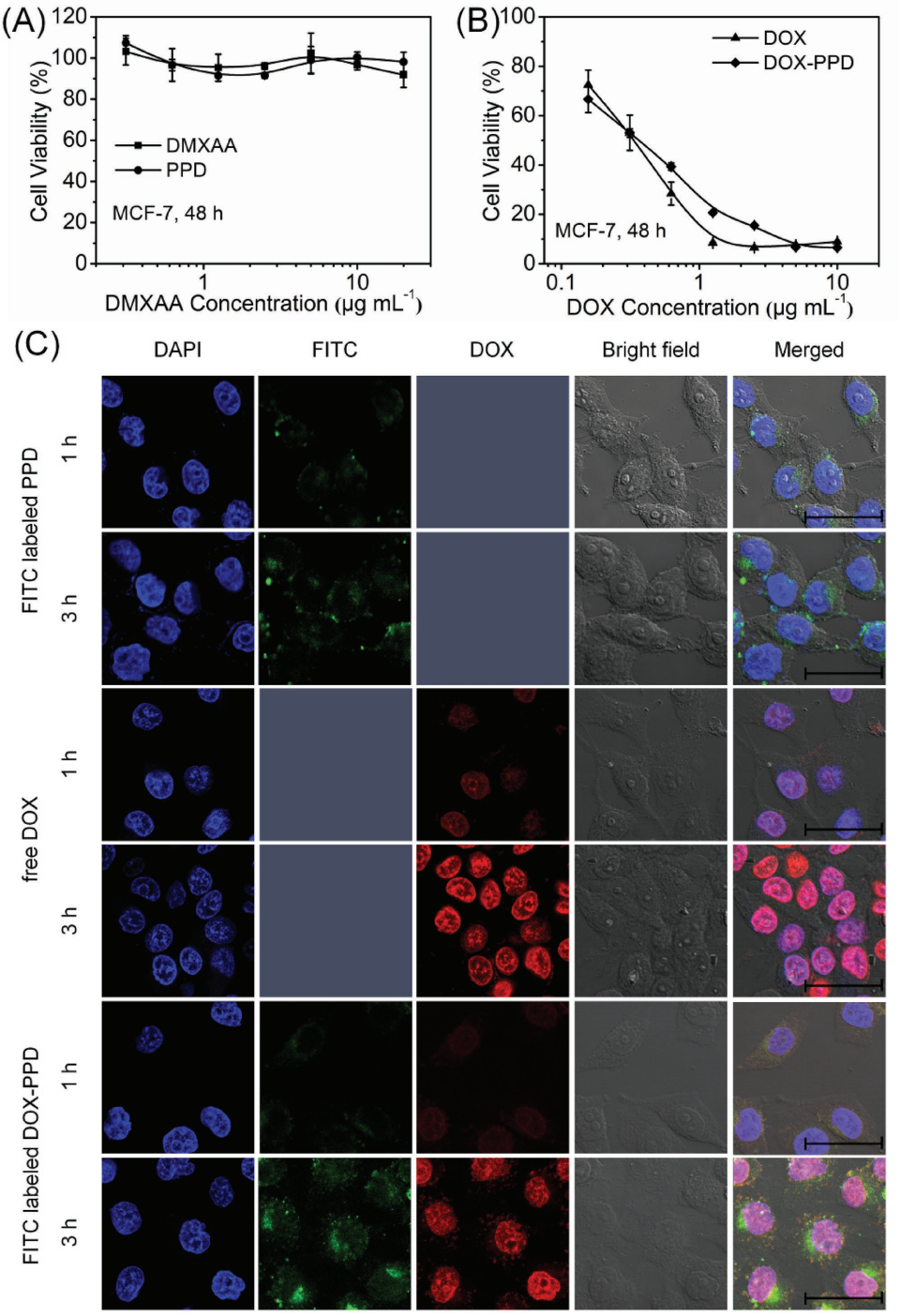

Figure 2. A,B) In vitro cytotoxicity of free DMXAA, PPD, free DOX, and DOX-PPD to MCF-7 cells. C) CLSM images of MCF-7 cells after incubation with FITC-labeled PPD, free DOX, and FITC-labeled DOX-PPD for 1 and 3 h (scale bar = 50 μm).

inhibition activity as compared with free DOX. The superior in vitro antitumor activity of DOX-PPD micelles was probably attributed to the efficient cell uptake and rapid DOX release in tumor cells triggered by intracellular lower pH condition.

The cellular uptake studies of PPD and DOX-PPD were performed with MCF-7 cells using confocal laser scanning microscopy (CLSM). The cellular nuclei were stained with 4′,6-diamidino-2-phenylindole dihydrochloride (DAPI), and PPD was labeled by fluorescein isothiocyanate (FITC) for the subcellular observation. CLSM images suggested that both PPD and DOX-PPD micelles could be taken up by tumor cells (Figure 2C). As compared with free DOX, DOX-PPD micelles showed comparative intracellular DOX fluorescence, indicating that DOX could be efficiently released from DOX-PPD micelles in the intracellular compartments after the micelles were taken up by tumor cells.

2.3. In Vivo Distribution of NP in Solid Tumor and Antitumor Activity Studies

One major issue in the antitumor drug delivery field is to transport a sufficient quantity of NMs to the entire tumor tissue for an effectively and thoroughly therapeutic outcome.[3,12] Toward this goal, tremendous effort has been put on developing tumor-penetrating NMs by controlling NM size or surface properties, and some progress has been made. However, even these well-designed NMs characterized with optimized sizes and surface properties cannot diffuse efficiently to the whole tumor region especially the central area of solid tumor tissues,[14–16] reflecting that the penetration of NMs to tumor tissues is not only just affected by their own properties, but also dominated by the tumor inherent abnormal features. Therefore, it is vital to find an alternative

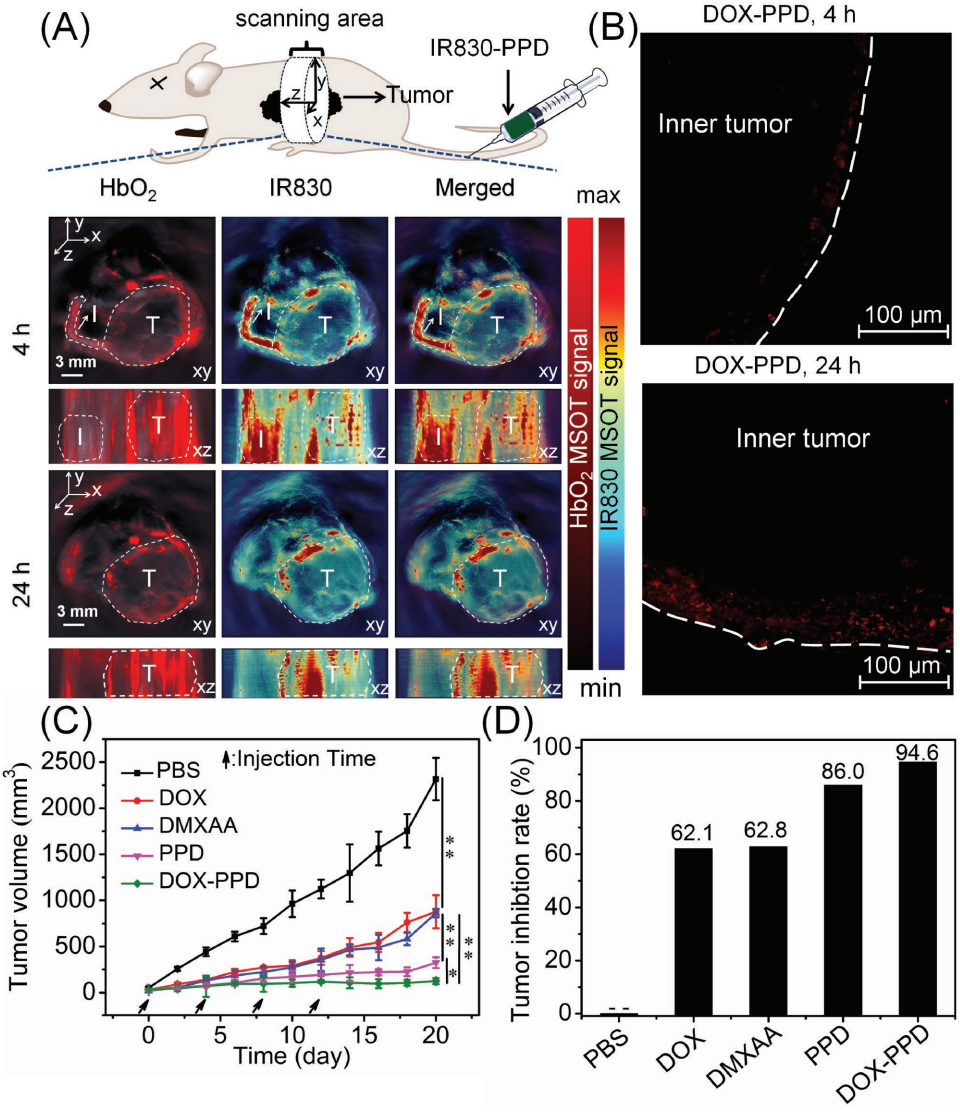

Figure 3. A) Orthogonal view of MSOT images of MCF-7 tumor bearing mice at 4 and 24 h after injection of IR830-PPD. "T" represents tumor regions, and "I" represents intestine. The HbO_2 images show the blood supply status of the mice. B) Antitumor drug distribution by excised DOX fluorescence at the implanted MCF-7 tumor. The tumor tissue slides were sectioned after 4 (upper) and 24 h (lower) postinjection of DOX-PPD and observed by CLSM. C) Tumor volume change of MCF-7 tumor bearing nude mice during the treatment, the dosages for DOX and DMXAA formulations were 5 and 10 mg kg^{-1}, respectively. The data are shown as mean ± SD ($n = 6$), *$p < 0.05$, **$p < 0.001$. D) Tumor inhibition rates of different formulations.

way to design the NMs that can display full-scale antitumor efficacy with no dependencies on tumor penetration. To accomplish this purpose, we hypothesized that NP containing a VDA and a chemotherapeutic agent could effectively inhibit tumor growth even if the NP could not penetrate into the entire tumor tissue. After expounding the theoretical feasibility of this hypothesis, we further designed a codelivery system of DMXAA and DOX to verify the hypothesis.

At first, we investigated the intratumor distribution of the designed NP. The study was performed by using an orthotopic solid tumor model which was generated by the subcutaneous injection of MCF-7 cells into the mammary fat pad of each mouse, and a multispectral optoacoustic tomographic (MSOT) technology was utilized to observe the NPs in vivo. PPD was first labeled by IR830 for the MSOT observation (Scheme 2C and Figure S8, Supporting Information). The MSOT test was performed at 4 and 24 h postinjection of IR830-PPD, and the scanning area was focused on the tumor region. IR830 and oxyhemoglobin (HbO_2) signals were both detected to visualize the NP and blood vessel distributions, respectively. The cross-section views of the tumors showed that IR830 signals were mainly located at the tumor periphery, but rarely observed in the tumor inner regions even at 24 h postinjection (**Figure 3**A), demonstrating that the NPs could hardly penetrate into the tumor inner regions. The HbO_2 signals revealed the heterogeneous distribution of blood vessels in the MCF-7 tumor (Figure 3A). A dense network of blood vessels was found only at the tumor periphery, while active vessels were lacking in the large central regions of the tumor which was consistent with the literatures.[42–44] Therefore, the heterogeneous intratumor vessels observed in the study may give direct evidence to explain why so many NMs with elaborately tailored particle size or surface properties only have restricted tumor penetration. It also could be found that NPs were distributed close to/around the blood vessels by comparing the colocation of IR830 and HbO_2 signals, further confirming that NPs cannot easily diffuse from the highly vascularized periphery to the avascular inner tumor tissues largely because of the elevated intratumoral interstitial fluid pressure.

Next, we tested the intratumoral distribution of the antitumor drugs delivered by NPs. DOX-PPD was injected intravenously to the mice bearing orthotopic MCF-7 tumors via tail vein, and intratumoral drug distribution was investigated through analyzing the DOX fluorescence in the tumor tissue by CLSM. As expected from the MOST study mentioned earlier, the CLSM images showed that the delivered drugs accumulated at the tumor periphery instead of penetrating into the inner tumor regions (Figure 3B). Combined with the MOST results, we could draw the conclusion that both NPs and the delivered drugs tended to accumulate at the highly vascularized tumor periphery, but had obvious limitations in penetrating into the avascular tumor central areas due to the tumor inherent features. Therefore, NMs containing traditional chemotherapeutic drugs may achieve enhanced tumor accumulation via EPR effect, while their overall efficiency will still be restricted as only partial exterior tumor cells are exposed to therapeutic agents. Thus, the combination of the nontumor penetrating NMs with VDAs, which can effectively inhibit the inner tumor cells just at the tumor rim, may become a compelling choice.

At last, we investigated whether the DMXAA and DOX codelivered NPs could display amplified therapeutic efficacy in treating solid tumors after confirming their incompetence in tumor penetration. For the antitumor study, mice bearing orthotopic MCF-7 breast tumors (initial tumor size was 30–50 mm^3 at day 0) were treated i.v. with free DOX, free DMXAA, PPD, and DOX-PPD four times on days 0, 4, 8, 12, and PBS was used as a control group. As shown in Figure 3C, the average tumor volume grew extremely fast in the PBS group, which reached to ≈2300 mm^3 on day 20, demonstrating the malignant growth of tumor cells. DOX and DMXAA showed moderate effect on tumor growth inhibition, and the tumor inhibition rates of the two groups were ≈60% (Figure 3D). PPD exhibited enhanced antitumor activity as compared to free DMXAA (tumor inhibition rate = 86.0%), which might be attributed to the suitable location nearby the tumor blood vessels (Figure 3A) and extended tumor vascular disrupting activity as mentioned in the release study. Eventually, DOX-PPD displayed the best antitumor activity with effective and permanent inhibition effect on tumor growth, and the tumor inhibition rate was as high as 94.6% (Figure 3C,D). Together with the tumor distribution study, the result verified that the NM containing VDA and cytotoxic drug was highly effective in inhibiting solid tumor growth even it could not penetrate into inner tumor tissues.

Body weight change was recorded as an indicator of systemic toxicity. The results showed that PPD or DOX-PPD did not lead to any obvious body weight decrease during the whole treatment (Figure S9, Supporting Information), revealing their excellent safety profiles.

3. Conclusions

In conclusion, we demonstrate an effective strategy to inhibit solid tumors by a nontumor penetrating NP containing chemotherapeutics and tumor-VDAs. By MSOT and CLSM imaging technique, we proved that solid tumor had a highly vascularized tumor periphery, while inner tumor regions lack vessels. NPs and the delivered drugs tend to accumulate mainly at tumor periphery rather than diffuse into tumoral inner regions, revealing limited antitumor effect by NPs delivered cytotoxic agent if the cancer cell killing depends on complete exposure to and direct contacting with the cytotoxic agent. While utilizing selective aggregation and long retention of NPs at the tumor rim, we hypothesize that NMs containing both VDAs and cytotoxic drugs may inhibit tumor growth effectively disregarding their tumor permeability. By releasing VDA and chemotherapeutic agent locally for each intended function, disruption of vascular network by VDA to starve the inner tumor cells remotely and killing of cancer cells in exterior regions of tumor tissue by chemotherapeutic agent, nontumor-penetrating NM may still effectively eradicate solid tumor. Through the in vivo studies, we demonstrate this hypothesis and confirm that the NP codelivering DMXAA and DOX display a vigorous inhibition effect on solid tumor growth even it cannot penetrate into tumor

tissues. This investigation demonstrates a simple but effective use of NMs to inhibit solid tumor growth without considering their tumor penetration profiles. Still, more investigations are needed to clarify the mechanisms of this combination strategy and whether the strategy can be effective against other solid tumors.

4. Experimental Section

Materials: Poly(ethylene glycol) monomethyl ether (mPEG, M_n = 5000) was purchased from Aldrich and used as received. mPEG-NH_2 was prepared according to the previous work.[45] BLA-NCA was synthesized according to the literature.[46] DMXAA and IR830-COOH were prepared in the laboratory. Doxorubicin hydrochloride (DOX·HCl) was purchased from Beijing Huafeng United Technology Corporation. *N*,*N*-dimethylformamide (DMF) was stored over calcium hydride (CaH_2) and purified by vacuum distillation with CaH_2 before use. MTT and DAPI were purchased from Sigma. FITC was purchased from Aladdin. Other reagents and solvents were purchased from Sinopharm Chemical Reagent Co. Ltd. and used as received.

Characterizations: The ^{1}H NMR, FT-IR, DLS, zeta potential, and TEM measurements were performed as described in the previous study.[47] Molecular weight distributions (PDI = M_w/M_n) of the copolymers were determined by GPC using the same test condition as given in the previous work.[48]

Synthesis of mPEG-b-PHEA Block Copolymer: mPEG-*b*-PBLA copolymer was synthesized through the ROP of the BLA-NCA monomer with mPEG-NH_2 as the macroinitiator. Briefly, mPEG-NH_2 (8.00 g, 1.6 mmol) was first dehydrated through an azeotropic process with toluene. The remaining toluene was removed under vacuum and then mPEG-NH_2 was dissolved in dry DMF (80 mL). Afterward, BLA-NCA (5.58 g, 22.4 mmol) dissolved in dry DMF (50 mL) was added into the above solution via a syringe under argon. The reaction was maintained at 35 °C under gentle stirring for 2 d. Then, acetic anhydride (1.6 mL, 16.9 mmol) was added to the solution and the mixture was maintained at 35 °C for another 12 h. The mixture was concentrated under vacuum at 60 °C. mPEG-*b*-PBLA copolymer was obtained by the repeated precipitation from DMF into excess amount of ice diethyl ether. Yield: 86%.

Subsequently, mPEG-*b*-PBLA (7.46 g, 1.0 mmol) was dissolved in dry DMF (100 mL), and then ethanolamine (3 mL) was added. The mixture was maintained at 35 °C under gentle stirring for 24 h. The mPEG-*b*-PHEA crude product was obtained by precipitation into excess amount of ice diethyl ether and dried under vacuum. Afterward, the crude product was placed into a dialysis bag (MWCO = 3500 Da) and dialyzed against distilled water. The purified mPEG-*b*-PHEA was obtained after lyophilization, yielding a white solid. Yield: 71%. ^{1}H NMR of mPEG-*b*-PBLA and mPEG-*b*-PHEA was measured using CF_3COOD as a solvent.

Synthesis of PPD: PPD was prepared through the condensation reaction of mPEG-*b*-PHEA and DMXAA using diisopropylcarbodiimide (DIC) as condensing agent and dimethylaminopyridine (DMAP) as catalytic agent. In brief, mPEG-*b*-PHEA (0.690 g, 0.1 mmol), DMXAA (0.367 g, 1.3 mmol), and DMAP (119 mg, 0.97 mmol) were added to a flame-dry flask and dissolved in dry DMF (10 mL) after vacuum for 12 h. Subsequently, DIC (1.31 g, 10.4 mmol) was added via a syringe. The reaction was maintained at 25 °C for 24 h. The solution was precipitated with excess amount of cold diethyl ether to remove unreacted DMXAA and other small molecules. The precipitation was repeated twice before pumping vacuum and PPD crude product was obtained. Then the crude product was dissolved in DMF and dialyzed against distilled water. The purified product was obtained as a white solid after freeze-drying. ^{1}H NMR of PPD was measured using DMSO-d_6 as a solvent. The DMXAA amount in the PPD conjugate was measured by UV–vis spectrometer at 343 nm.

FITC-labeled PPD was prepared as described in the previous work.[7] Briefly, PPD (50.0 mg) and FITC (2.5 mg) were dissolved in DMF (2.0 mL) and the reaction solution was stirred for 24 h at room temperature in dark. Then the mixture was dialyzed against distilled water and freeze-dried. The FITC-labeled PPD yellow powder was obtained after lyophilization and stored at the dark place.

Preparation of DOX-PPD: DOX-PPD NPs were prepared by a nanoprecipitation technique.[49] Typically, the lyophilized PPD powder (100 mg), DOX·HCl (7.0 mg), and triethylamine (2.5 mg) were mixed in DMF (4.0 mL). The mixture solution was maintained at 25 °C for 6 h in the dark, and then added dropwise into distilled water (10 mL) under vigorously stirring. The mixture was stirred in the dark for another 12 h. DMF and other small molecules were removed by sufficient dialysis (MWCO 3500 Da) against distilled water. DOX-PPD NPs were obtained after lyophilization. To determine DOX content in DOX-PPD, DOX-PPD was dissolved in DMF and measured by UV–vis spectrometer at 480 nm. Drug loading content (DLC, wt%) and drug loading efficiency (DLE, wt%) were calculated according to the following formula

$$\mathrm{DLC} = \left(\frac{\text{amount of loaded drug}}{\text{amount of drug loaded NPs}}\right) \times 100\% \quad (1)$$

$$\mathrm{DLE} = \left(\frac{\text{amount of loaded drug}}{\text{amount of feeding drug}}\right) \times 100\% \quad (2)$$

DOX loaded FITC-labeled PPD (FITC-labeled DOX-PPD) NPs were also prepared through the same procedure described above.

To estimate the stability of PPD and DOX-PPD in plasma, PPD and DOX-PPD were dissolved in PBS containing 10% FBS, and then the solutions were placed in a thermotank at 37 °C under gently shaking at 100 rpm. At designed time intervals (4, 12, 24, 48, and 72 h), a small quantity of the solution was withdrawn and followed by DLS measurement.

In Vitro Drug Release Study: The in vitro drug release was investigated in PBS. Briefly, the weighted PPD or DOX-PPD powder was dissolved in 5.0 mL of release medium and placed into a dialysis bag (MWCO 3500 Da). Then the dialysis bag was transferred into 45.0 mL of release medium. The release study was performed in a thermotank under gently shaking at 100 rpm at 37 °C. At desired time intervals, 4 mL of release solution was withdrawn and replaced with equal amount of fresh release medium. The DMXAA and DOX release amount were determined by UV–vis spectrometer at 343 and 480 nm, respectively.

Cell Cultures: The human lung carcinoma A549 cells, breast carcinoma MCF-7 cells, and mouse embryo fibroblast NIH/3T3 cells were cultured in Dulbecco's modified Eagle's medium (DMEM) with high glucose containing 10% FBS, supplemented with 50 U mL^{-1} penicillin and 50 U mL^{-1} streptomycin, and incubated at 37 °C in 5% CO_2 atmosphere.

In Vitro Cytotoxicity Study: The in vitro cytotoxicities of mPEG-*b*-PHEA, free drugs, PPD, and DOX-PPD were investigated by MTT assay. Briefly, A549, MCF-7 or NIH/3T3 cells were seeded in 96-well plates at 7000 cells per well in 100 µL of DMEM medium and incubated at 37 °C in a 5% CO_2 atmosphere for 24 h. Subsequently, the original culture medium was removed and replaced with 200 µL fresh DMEM containing mPEG-*b*-PHEA, free DMXAA, PPD, free DOX, and DOX-PPD at the different concentrations. After 48 h incubation, the cells were subjected to MTT assay. The absorbency of the solution was measured on a Bio-Rad 680 microplate reader at 492 nm. The relative cell viabilities were calculated by the following equation: (*A* sample/*A* control) × 100, where *A* sample and *A* control represented the absorbances of the sample well and control well, respectively. Data are presented as means ± SD ($n = 3$).

CLSM Study: The cellular uptake behaviors of FITC-labeled PPD and DOX-PPD were investigated by CLSM toward MCF-7 cells. The cells were seeded on the coverslips in 6-well plates with a density of 1×10^5 cells per well and incubated for 24 h, and then the original medium was replaced with FITC-labeled PPD, free DOX or FITC-labeled DOX-PPD (at a DOX concentration of 5 µg mL^{-1} in 2 mL of DMEM). The culture media were removed after 1 or 3 h incubation. The cells were washed with fresh PBS and fixed with formaldehyde (4% in PBS) for 20 min at room temperature. Then the cell nuclei were stained by DAPI. The coverslips were placed onto the glass microscope slides. The subcellular localizations of FITC-labeled PPD and DOX-PPD were visualized under a laser scanning confocal microscope (Carl Zeiss LSM 780).

MSOT Test: The intratumor distribution of NP was investigated by MSOT measurement. For MSOT observation, PPD was first labeled by IR-830, a near-infrared fluorescence dye. In brief, PPD (200 mg), IR830-COOH (34 mg), and DMAP (6.1 mg) were added to a flame-dry flask and dissolved in dry DMF (5 mL). Subsequently, DIC (31.5 mg) was added via a microsyringe. The reaction was maintained at 25 °C for 24 h. The solution was precipitated with excess amount of cold diethyl ether to remove unreacted small molecules. Afterward, the crude product was dissolved in DMF and dialyzed against distilled water, the purified IR830-labeled PPD (IR830-PPD) was obtained as a dark green powder after freeze-drying.

The optoacoustic imaging was carried out on a MSOT scanner equipped with 128 ultrasound transducer elements (MSOT inVision 128, iThera Medical GmbH, Munich, Germany). Female BALB/c nude mice bearing MCF-7 orthotopic tumor were injected with IR830-PPD NPs via tail vein. At the designed time intervals (4 and 24 h), the mice were anesthetized with 2% isoflurane and placed into the MSOT system, multispectral process scanning was performed at 680, 750, 815, 825, 850, and 900 nm. The results were reconstructed in a linear model, and the multispectral processing was carried out in linear regression.

Excised CLSM Imaging: To investigate the intratumor drug distribution, female BALB/c nude mice bearing orthotopic MCF-7 tumor (100–200 mm^3) were injected with a single dose of DOX-PPD NPs (15 mg DOX kg^{-1}) via tail vein. After 4 and 24 h, the mice were sacrificed. The tumors were collected and embedded in Tissue-Tek OCT embedding medium. Cryogenic slides (10 µm in thickness) were performed by a freezing microtome (Leica CM 1900) and placed on polylysine-coated glass slides (Wuhan Boster AR1065). The tumor sections were fixed in paraformaldehyde (4% in PBS) at room temperature for 15 min. After washing with PBS for three times, the tumor sections were stained with DAPI, and then observed under a confocal laser scanning microscope (Carl Zeiss LSM 780).

In Vivo Antitumor Study on Orthotopic Xenograft Model: The in vivo antitumor studies were performed on mice bearing orthotopic human breast tumor. Female BALB/c nude mice were maintained in specific pathogen free animal lab and used under the approval of the Animal Care and Use Committee of Jilin University. The xenograft tumor model was generated by the subcutaneous injection of MCF-7 cells (1.5×10^6) into the mammary fat pad of each mouse. When the tumor volume reached ≈50 mm^3, the mice were randomly divided into five groups and the treatment was started, and this day was designated as day 0. Mice were treated with PBS, free DOX·HCl (5 mg kg^{-1}), free DMXAA (10 mg kg^{-1}), PPD (10 mg DMXAA kg^{-1}), and DOX-PPD (5 mg DOX kg^{-1} and 10 mg DMXAA kg^{-1}) on days 0, 4, 8, and 12. The treatments were performed through intravenous injection via tail vein. Tumor volumes were measured every other day by a vernier caliper as indicators to assess the antitumor activities, and body weights were measured simultaneously to observe systematic toxicities. The tumor volume (mm^3) and tumor suppression rate (%) were calculated according to the following equations

$$\text{Tumor volume}(V) = a \cdot b^2/2 \tag{3}$$

$$\text{Tumor inhibition rate} = \left[\left(W_c - W_x\right)/W_c\right] \times 100\% \tag{4}$$

a and *b* represented the longest and shortest diameter of the tumors respectively. W_c represented the average volume of tumors in the control group, and W_x represented the average volume of tumors in the treatment group.

Statistical Analysis: All experiments were performed at least three times and expressed as means ± SD. Statistical significances were analyzed using the Student's *t*-test. $P < 0.05$ was considered statistically significant, and $P < 0.01$ was considered highly significant.

Supporting Information

Supporting Information is available from the Wiley Online Library or from the author.

Acknowledgements

This research was financially supported by the National Natural Science Foundation of China (Project Nos. 51173184, 51373168, 51021003, 51233004, 51321062, and 51403204), Ministry of Science and Technology of China (International Cooperation and Communication Program 2011DFR51090), and the Program of Scientific Development of Jilin Province (20130206066GX and 20130727050YY). The authors declare no competing financial interest.

[1] M. E. Davis, Z. Chen, D. M. Shin, *Nat. Rev. Drug Discovery* **2008**, *7*, 771.
[2] Y. H. Bae, K. Park, *J. Controlled Release* **2011**, *153*, 198.
[3] X. Q. Zhang, X. Xu, N. Bertrand, E. Pridgen, A. Swami, O. C. Farokhzad, *Adv. Drug Delivery Rev.* **2012**, *64*, 1363.
[4] F. Zhang, S. Zhang, S. F. Pollack, R. Li, A. M. Gonzalez, J. Fan, J. Zou, S. E. Leininger, A. Pavia-Sanders, R. Johnson, L. D. Nelson, J. E. Raymond, M. Elsabahy, D. M. P. Hughes, M. W. Lenox, T. P. Gustafson, K. L. Wooley, *J. Am. Chem. Soc.* **2015**, *137*, 2056.
[5] H. Cabral, M. Murakami, H. Hojo, Y. Terada, M. R. Kano, U-i. Chung, N. Nishiyama, K. Kataoka, *Proc. Natl. Acad. Sci. USA* **2013**, *110*, 11397.
[6] K. Osada, H. Cabral, Y. Mochida, S. Lee, K. Nagata, T. Matsuura, M. Yamamoto, Y. Anraku, A. Kishimura, N. Nishiyama, K. Kataoka, *J. Am. Chem. Soc.* **2012**, *134*, 13172.
[7] S. Lv, Z. Tang, M. Li, J. Lin, W. Song, H. Liu, Y. Huang, Y. Zhang, X. Chen, *Biomaterials* **2014**, *35*, 611829.
[8] W. She, K. Luo, C. Zhang, G. Wang, Y. Geng, L. Li, B. He, Z. Gu, *Biomaterials* **2013**, *34*, 1613.
[9] J. Yang, W. Liu, M. Sui, J. Tang, Y. Shen, *Biomaterials* **2011**, *32*, 9136.
[10] J.-Z. Du, X.-J. Du, C.-Q. Mao, J. Wang, *J. Am. Chem. Soc.* **2011**, *133*, 17560.
[11] L. Yu, T. Ci, S. Zhou, W. Zeng, J. Ding, *Biomater. Sci.* **2013**, *1*, 411.
[12] J. W. Nichols, Y. H. Bae, *J. Controlled Release* **2014**, *190*, 451.
[13] H. Cabral, Y. Matsumoto, K. Mizuno, Q. Chen, M. Murakami, M. Kimura, Y. Terada, M. R. Kano, K. Miyazono, M. Uesaka, N. Nishiyama, K. Kataoka, *Nat. Nanotechnol.* **2011**, *6*, 815.
[14] L. Tang, X. Yang, Q. Yin, K. Cai, H. Wang, I. Chaudhury, C. Yao, Q. Zhou, M. Kwon, J. A. Hartman, I. T. Dobrucki, L. W. Dobrucki, L. B. Borst, S. Lezmi, W. G. Helferich, A. L. Ferguson, T. M. Fan, J. Cheng, *Proc. Natl. Acad. Sci. USA* **2014**, *111*, 15344.
[15] L. Tang, T. M. Fan, L. B. Borst, J. Cheng, *ACS Nano* **2012**, *6*, 3954.
[16] L. Tang, N. P. Gabrielson, F. M. Uckun, T. M. Fan, J. Cheng, *Mol. Pharm.* **2013**, *10*, 883.
[17] D. Fukumura, R. K. Jain, *J. Cell. Biochem.* **2007**, *101*, 937.
[18] M. Kanapathipillai, A. Brock, D. E. Ingber, *Adv. Drug Delivery Rev.* **2014**, *79–80*, 107.
[19] M. Cesca, F. Bizzaro, M. Zucchetti, R. Giavazzi, *Front. Oncol.* **2013**, *3*, 259.
[20] D. Hanahan, R. A. Weinberg, *Cell* **2011**, *144*, 646.
[21] D. W. Siemann, *Cancer Treat. Rev.* **2011**, *37*, 63.
[22] J. W. Lippert 3rd., *Bioorg. Med. Chem.* **2007**, *15*, 605.
[23] F. Marcucci, A. Corti, *Adv. Drug Delivery Rev.* **2012**, *64*, 53.
[24] H. Maeda, J. Wu, T. Sawa, Y. Matsumura, K. Hori, *J. Controlled Release* **2000**, *65*, 271.
[25] H. Maeda, G. Y. Bharate, J. Daruwalla, *Eur. J. Pharm. Biopharm.* **2009**, *71*, 409.
[26] C. Yang, M. Bian, Z. Yang, *Biomater. Sci.* **2014**, *2*, 651.
[27] H. Qian, X. Wang, K. Yuan, C. Xie, W. Wu, X. Jiang, L. Hu, *Biomater. Sci.* **2014**, *2*, 220.
[28] C. J. Lash, A. E. Li, M. Rutland, B. C. Baguley, L. J. Zwi, W. R. Wilson, *Br. J. Cancer* **1998**, *78*, 439.
[29] G. G. Dark, S. A. Hill, V. E. Prise, G. M. Tozer, G. R. Pettit, D. J. Chaplin, *Cancer Res.* **1997**, *57*, 1829.
[30] D. W. Siemann, A. M. Rojiani, *Int. J. Radiat. Oncol.* **2002**, *53*, 164.
[31] L. Y. Li, A. Rojiani, D. W. Siemann, *Int. J. Radiat. Oncol.* **1998**, *42*, 899.
[32] A. M. Rojiani, L. Li, L. Rise, D. W. Siemann, *Acta Oncol.* **2002**, *41*, 98.
[33] Y. Bae, K. Kataoka, *Adv. Drug Delivery Rev.* **2009**, *61*, 768.
[34] M. Hughes, S. Debnath, C. W. Knapp, R. V. Ulijn, *Biomater. Sci.* **2013**, *1*, 1138.
[35] Y. Yue, C. Wu, *Biomater. Sci.* **2013**, *1*, 152.
[36] X. P. Duan, Y. P. Li, *Small* **2013**, *9*, 1521.
[37] T. Breidahl, F. U. Nielsen, H. Stodkilde-Jorgensen, R. J. Maxwell, M. R. Horsman, *Acta Oncol.* **2006**, *45*, 306.
[38] R. Murata, J. Overgaard, M. R. Horsman, *Int. J. Radiat. Biol.* **2001**, *77*, 195.
[39] M. Wankhede, C. Dedeugd, D. W. Siemann, B. S. Sorg, *Oncol. Rep.* **2010**, *23*, 685.
[40] Y. Wang, G. Wu, X. Li, Y. Wang, H. Gao, J. Ma, *Biomater. Sci.* **2013**, *1*, 614.
[41] P. M. LoRusso, S. A. Boerner, S. Hunsberger, *J. Clin. Oncol.* **2011**, *29*, 2952.
[42] J. W. Baish, T. Stylianopoulos, R. M. Lanning, W. S. Kamoun, D. Fukumura, L. L. Munn, R. K. Jain, *Proc. Natl. Acad. Sci. USA* **2011**, *108*, 1799.
[43] J. Holash, S. J. Wiegand, G. D. Yancopoulos, *Oncogene* **1999**, *18*, 5356.
[44] B. A. Graff, I. C. Benjaminsen, K. G. Brurberg, E. B. Ruud, E. K. Rofstad, *J. Magn. Reson. Imaging* **2005**, *21*, 272.
[45] H. Y. Tian, C. Deng, H. Lin, J. R. Sun, M. X. Deng, X. S. Chen, X. B. Jing, *Biomaterials* **2005**, *26*, 4209.
[46] A. Harada, K. Kataoka, *Macromolecules* **1995**, *28*, 5294.
[47] S. X. Lv, M. Q. Li, Z. H. Tang, W. T. Song, H. Sun, H. Y. Liu, X. S. Chen, *Acta Biomater.* **2013**, *9*, 9330.
[48] M. Li, S. Lv, Z. Tang, W. Song, H. Yu, H. Sun, H. Liu, X. Chen, *Macromol. Biosci.* **2013**, *13*, 1150.
[49] S. X. Lv, W. T. Song, Z. H. Tang, M. Q. Li, H. Y. Yu, H. Hong, X. S. Chen, *Mol. Pharm.* **2014**, *11*, 1562.

Received: March 19, 2016
Revised: November 27, 2016
Published online: January 12, 2017

